Monitoring Structural Variation on Gd Ratio of La Modified Bismuth Ferrite Ceramics with Enhanced Magnetization

Mehmet S. Bozgeyik[*1, 2, 3], Nurvet Kirkgecit[3], Rajesh K. Katiyar[1], and Ram S. Katiyar[1]

[1] Department of Physics and Institute for Functional Nanomaterials, University of Puerto Rico, San Juan, Puerto Rico 00931-3334, USA

[2] Department of Physics, Faculty of Science and Literature, Kahramanmaras Sutcu Imam University, Kahramanmaras, 46100, TURKEY

[3] Department of Materials Science and Engineering, Graduate School of Natural and Applied Science, Kahramanmaras Sutcu Imam University, Kahramanmaras, 46100, TURKEY

[*] Corresponding author: email address: msbozgeyik@yahoo.com (Mehmet S. Bozgeyik)

ABSTRACT

Critical structural variation and dielectric properties were investigated in Lanthanum and Gadolinium co-substituted bismuth ferrite ($Bi_{0.9}La_{0.1}Fe_{1-x}Gd_xO_3$ (x=0.01, 0.03, 0.05, 0.07, 0.1, and 0.15). Conventional solid state reaction technique was used to synthesize ceramic samples. To investigate the influence of co-substitution on the phase formation and crystal structure, X-ray diffraction method (XRD), Scanning electron microscopy (SEM) and Raman spectroscopy were utilized. Probing the structural properties by changing Gd ratio was carried out to ensure single phase of rhombohedral R3c structure. Hence, the exploration of dielectric properties of single phase modified $BiFeO_3$ (BFO) ceramic was executed by room temperature capacitance and loss tangent measurements. It was found that by substitution of

10 mol% La for Bi and up to 5 mol% Gd for Bi, perovskite structure of rhombohedral symmetry and R3c space group were formed. This possessed enhanced magnetization and reduced dielectric loss compared to pure BFO.

Keywords: Ceramics; Solid state reaction; Crystal structure; Microstructure; Magnetisation; Dielectric response;

1. Introduction

Materials having ability to exhibit two or more ferroic orders of ferromagnetic (or antiferromagnetic), ferroelectric, ferroelastic, and ferrotoroid simultaneously are called as multiferroics (MF). These are functional intelligent materials. Magnetoelectric effect described as cross coupling between electric and magnetic fields is needed to defined here to magnify the function of magnetoelectric multiferroics. Those simultaneously have both ferroelectric (electric dipole moment) and ferro/antiferro-magnetic (magnetic moment) order parameters. Magnetoelectric multiferroics (ME-MF) supply a unique occasion to employ distinct functionalities in a single material. Clearly, this function makes it feasible to provoke polarization by external magnetic field and magnetization by applied electric field. Hence, above capabilities make magnetoelectric multiferroics potential materials in novel device applications such as spintronics [1], non-volatile memories [2], consumer electronics, etc.[2-8]. Perovskite-oxides offer many multiferroic materials like bismuth ferrite (BiFeO3) [9], yttrium manganate (YMnO3) [10].

Among the single phase magnetoelectric multiferroics bismuth ferrite ($BiFeO_3$) is unique at room temperature. Bulk $BiFeO_3$ is a G-type antiferromagnetic which possess Neel temperature at 655 K and a high Curie temperature at 1043 K [11]. Therefore, this material has drawn huge attention for widespread technology as well as scientific interest. However, BFO has some application problems namely, poor insulation and weak magnetization. These

two mainly reduce the magnetoelectric coupling [12]. Thus, $BiFeO_3$ related researches were mainly devoted on solving these issues. As a matter of fact, crystal lattice of bulk $BiFeO_3$ has a perovskite structure which is rhombohedrally distorted and has a R3c space group [12]. Constituent Bi^{3+} and Fe^{3+} cations remove along $(111)_c$ direction. Meantime, oxygen octahedral enclosing these ions rotate about this direction alternately clockwise and counterclockwise [13, 14]. Physical mechanism underneath the ferroelectric and poor insulation properties is as follows: Ferroelectricity is originated from bismuth ions. Stereochemically active bismuth $6s^2$ lone pair electrons with its empty $6p^0$ orbital and $2p^6$ orbital of oxygen are hybridized. Additionally, the relative movements of Bi^{3+} and Fe-O octahedron along the $(111)_c$ direction cause for electric polarization [15-17]. Essentially, oxygen vacancies created by bismuth deficiencies are common space charge defects in such perovskite structures. Application of electric field causes these charges to accumulate into domain walls, grain boundaries, and interfaces which have lower energies [18], so inevitably leakage current appears through material. Another shortcoming about bismuth ferrite is the weak insulation due to the leakage current. The main sources of this problem are bismuth deficiencies and mixed valance states of Fe^{3+} and Fe^{2+}. As a result, oxygen vacancies result in such a high leakage current which yields for high dielectric losses. These problems decrease the reliability of bismuth ferrite in potential device applications [6, 16, 19]. Hence, ferroelectricity is restricted by leakage current by pinning on domain walls. Moreover, this mechanism hinders implementation due to poor multiferroic and magnetoelectric properties [20-22]. Physics of magnetism mechanism in $BiFeO_3$ is as follows: Due to Jahn-Teller structural distortion magnetic moments of partially filled 3d orbitals of Fe^{3+} ions are antiferromagnetically coordinated in G-type form. In fact, within (111) planes magnetic moments are paired ferromagnetically but between neighboring planes they are antiferromagnetically aligned [23, 24]. Additionally, antiferromagnetic layout has spatially

long range cyloidal spin structure due to the rotation of canted magnetic moments in the (110) direction with incommensurate 62 nm period [25-27]. Remaining magnetic moment and linear magnetoelectricity vanish in the cycle period. Consequently, no net magnetization remains through the material. As a result, this mechanism restricts the linear magnetoelectric effect. On the contrary, once this cycloid structure of spins is avoided, slightly canted magnetic moment perpendicular to the rhombohedral axis results in a minor macroscopic magnetization, viz. weak ferromagnetism [19].

Based on the material reality and above problems, to improve multiferroic and magnetoelectric properties for device implementation it is highly desirable to boost the magnetization and diminish the leakage current. To do so, it is required to somehow eliminate the sources of the problems and alternate the causative or provoking mechanisms in convenient approaches. Regarding magnetism, for instance, suppression of the spin cycloid structure would be possible by fabricating nanoparticle in size smaller than 62 nm, and consequently it would give rise to induction of ferromagnetism by means of uncompensated canted magnetic moments. Variety methods are conducted to increase magnetization and insulation properties. Concerning to collapse of spin cycloid structure and improve magnetism, for instance, recalling the ABO_3 perovskite structure A-site and/or B-site ion substitutions [28] are widespread approaches [29]. Moreover, this way also diminishes leakage current that appears ferroelectricity [30-32]. Consequently, appropriate substitutions would enhance the multiferroic and magnetoelectric properties and thereby lead to device applications [33]. In this context, recalling volatility problem of Bi comparatively more stable Lanthanum (La) substitution would avoid creation of Bi and oxygen vacancies. As a result, leakage current would be lowered in same part by holding electric polarization [34].

Since the ultimate goal is to improve multiferroic properties of BFO, the motivation underneath the current research is to destroy the spin cycloid structure via deformation of the

crystal structure. We hope to create certain distortion and twist in the perovskite structure by substitutions of cooperatively large Gd ion for Fe and small La ion for Bi. Moreover, due to the fact that Gd magnetic moment is higher than that of Fe, inequality of antiparallel magnetization of sublattice and diversity of Fe-O-Fe_{Gd} bond angle and bond length will cause to alter spin cycloid structure. Therefore, the spin cycloid structure will probably give rise to net magnetization different than zero and thereby results to increase linear magnetoelectric constant. Furthermore, compared to Bi more stable La substitution utilizes the low dielectric loss and improve magnetization [34] as well as diminish impurity phases [35], etc. Also magnetic properties of BFO could be expected to improve with magnetic properties of Gadolinium. With 0.938 nm ionic radius Gd [36] (against to 0.55 nm for Fe) [37]) has a potential to destroy the cycloidal spin structure and induce ferromagnetism via avoid equality between magnetic moments of sublattices. Additionally, regarding Fe-O-Fe_{Gd} the difference of bond parameters will give rise enhanced magnetization.

2. Experimental details

2.1 Samples Preparation

Solid-state reaction route is utilized to synthesize polycrystalline $Bi_{0.9}La_{0.1}Fe_{1-x}Gd_xO_3$ (x=0.01, 0.03, 0.05, 0.07, 0.10, and 0.15) ceramics. Stoichiometric ratios of high grade oxide precursors of Bi2O3 (Puratronic, 99.999%), La2O3 (REacton, 99.999%), Fe2O3 (Puratronic, 99.998%), and Gd2O3 (REacton, 99.99%) were used. As a matter of fact Bi is a volatile compound above 800 °C, to compensate Bi loss during calcination and sintering processes the amount of Bi_2O_3 is increased 5 mol%. Hence, to avoid Bi loss (A-site vacancies) 10 mol% La is fixed since La is more stable than Bi. Since the La ratio is fixed we labeled the samples with respect to Gd ratio ranging from 0 to 15 as 0-15 Gd. First of all, high energy ball milling process mixed the oxide precursors for 16 h in methanol medium. After drying on a hot plate at 90 °C the mixed row powder was calcined in box furnace at 850 °C for 4 h in air. Later,

calcined bulk ceramics were gently milled and mixed with polyvinyl alcohol (PVA) in an agate mortar for a while. Next, a hydraulic press is utilized to form pellets by applying isostatic pressure. Eventually, the pellet ceramics were sintered at 850 $^{\circ}$C for 4 h in atmosphere.

2.2 Characterization techniques

Initial structural analysis was carried out to study the crystal structure by X-ray diffraction (XRD) technique. Surface microstructures were studied by scanning electron microscope (SEM). Structure is also studied by Raman spectroscopy of Horiba Jobin Yvon T64000. Dielectric response was recorded by an impedance analyzer HP4294A in a wide frequency range of 100 Hz to 1 MHz at room temperature. Magnetic characterization was examined by operating Vibration Sample Magnetometry (VSM).

3. Results and discussion

3.1 Crystal structure and microstructure analysis

Effects of La-Gd co-substitution on the crystal structure properties studied by XRD are presented in Figure 1. All samples are completely crystallized in polycrystalline forms. Due to the intense peaks match with those of parent $BiFeO_3$ they are labeled according to JCPDS-82-1254 as a perovskite structure of rhombohedral crystal system with R3c space group. Up to 5 mol% Gd the samples presents negligible bismuth deficient secondary phase of tetragonal $Bi_{25}FeO_{40}$ according to JCPDS card file no 46-0416. Overall observation is briefly expressed as that increasing Gd ratio causes to confederation of doubly split peaks by forming broaden one and partition of split into two peaks. Monitoring such evaluation of peaks indicates the crystal structure transformation. Merging of doublet peaks of (104)/(110), (006)/(202), (116)/(122), and (214)/(300) indicates the crystal structure transformation from rhombohedral

to orthorhombic by rising Gd ratio. By 3 mol% Gd substitution, partial structural transition initiate. As shown in the magnified part of XRD patterns in Figure 2, essentially, the doublet peaks of (104)/(110), (006)/(202), (116)/(122), and (214)/(300) are merging with increase of Gd ratio. Further increase of Gd concentration leads to split double peaks which indicate the structural transition. It is noted that these peaks shift to higher angle. Additionally, more impurity phases of orthorhombic $Bi_2Fe_4O_9$ with JCPDS card file no 74-1098 and cubic $Bi_{36}Fe_2O_{57}$ with JCPDS card file no 42-0181 are formed. Increasing the amount of secondary phases indicates that the Gd is no more substituted for Fe sites. Large ionic size difference between Gd and Fe ions cause lattice strain, distortion and structural disorders. Consequently, the nucleation rate is degraded [38]. Therefore, grain size decrease with increase of Gd ratio as shown in the microstructure in Figure 3. Clear, dense and almost homogenous grain growth was observed for 0 Gd and 1 Gd samples. Sharp grain boundaries lead to distinguish each grain. By increasing the Gd ratio grain formation is strictly changed by means of size and form.

3.2 Raman spectroscopy

Influence of La-Gd co-substitutions of for Bi-Fe sites was further studied by Raman spectroscopy. In fact, as a nondestructive tool Raman spectroscopy is sensitive to structural variation by compositional disorders and local symmetry changes. Figure 4 shows the comparison of Raman spectra at room temperature upon related co-substituted $BiFeO_3$ with pure one. Based on group theory, theoretically, perovskite crystal $BiFeO_3$, having rhombohedral system and R3c space group, has thirteen Raman modes. Those of four are A_1 and nine of them are E modes. Practically, in our work, six of these modes are clearly observed but the rest of the modes are not detected due to the weak polarizability, mode broadening, accidental degeneracies. Figure 4 presents the both detected modes of E-1, E-2, E-3 and A_1-1, A_1-2, A_1-3, as well as the traces of unclear modes of E-4, E-5, E-6, E-7, E-8

and A_1-4 at possible wavenumbers. E-1, A_1-1, A_1-2, A_1-3, E-2, and E-3 peaks are measured following numbers of 75, 138, 173, 218, 261, and 287 cm^{-1}, respectively. In a $BiFeO_3$ perovskite structure, A_1 modes are related with the bismuth ion vibration in the structure [39]. E-1, E-2, and E-3 modes are raised from the vibration of Fe-O octahedral [39]. It is observed that La and Gd substitution causes to shift related peaks. Raman spectral changes are critically affected by structural changes, chemical bonds and symmetry. Moreover, stress and temperature cause to shift peak positions. For example, shift to higher wavenumbers is observed for the modes of A_1-1, A_1-2, and A_1-3. Since La is lighter than Bi, motion of La increases. Such ionic differences between La and Bi lead to twist the structure via shrinkage of the bond and reduced mass. Therefore, La substitution causes to shift A_1 modes to higher wavenumbers and peak broadening. Twist of lattice and oxygen octahedrons cause to decrease peak intensities. On the contrary, E-1, E-2, and E-3 modes are shifted to lower wavenumbers. Actually, atomic mass of Gd ion is bigger than that of Fe ions. As expected, the vibration frequencies of Gd-O bond decreases compared to that of Fe-O bond. Higher ionic radii and atomic mass cause to lattice distortion and oxygen octahedrals. Therefore, the peak intensities decrease with increasing Gd ratio. Those are the reason for disappearance of other six modes which are labeled at possible wavelengths in Figure 4.

3.3 Dielectric properties

Generally, dielectric properties depend on crystal structure, frequency of electric field, and temperature. Figure 5 presents the dielectric responses of the specimens by increasing frequency. Dielectric constant of La and Gd substituted samples are significantly decreased due to low polarizability. Smaller grain size upon La and Gd also contributes to decrease dielectric constant by increasing the density of insulating grain boundary. The general trend of relative dielectric permittivity (dielectric constant) is reduction by enhancing frequency due to the dielectric relaxation. Accordingly, at low frequencies dielectric dispersion is explained as

that the dipoles are capable to be arranged in the electric field. So, they contribute to the dielectric constant. On the contrary, increasing frequency does not allow dipoles to be arranged along the field. In this manner, relative dielectric permittivity decreases with improving frequency. Overall dielectric response indicates that high dielectric permittivity is high at low frequency but low at elevated frequencies. Dipole relaxation occurs in the system. This is a result of typical interface polarization of Maxwell-Wagner [40, 41]. Actually, polarization types of electronic, atomic, interfacial, and ionic participate in dielectric response at short frequencies. Moreover, space charge polarization and interface related polarization mechanisms are predominant at initial frequency range. At high frequencies, nevertheless, electrons are solely capable to follow the frequency of the field. At such frequencies space charges do not contribute to the permittivity. Therefore, it is significantly decreased with increased frequency.

Response of the energy dissipation factor (dielectric loss tanδ) with respect to frequency is plotted in Figure 6. Significant decrease of loss tanδ of La and Gd substituted samples is partially attributed to enhance of the insulating grain boundaries via decreasing grain size. It is observed that tanδ of BFO initially decreased than increased. On the other hand, that of 1 Gd decreases through all frequency range. Bismuth and oxygen ion vacancies are mobile space charges which are driven by the applied electric field to contribute the dielectric properties in the sample. However, they are not able to response to the electric field at higher frequencies, and consequently dielectric relaxation occurs accompanied by decrease dielectric constant and loss [40]. The observed peaks are the polarization resonances of the dipoles of such charged defects [40, 42]. Due to the above mechanism dielectric constant and loss of Gd substituted samples are evidently degraded compared to those of BFO (0 Gd). The observed peaks of loss tanδ indicate the dielectric relaxation. Upon La and Gd substitution this peak appears at lower frequency range compared to BFO. Generally, low dielectric

constant is because of low conductivity (high resistivity) and thereby decreases the dielectric loss [43]. Significant decrease of dielectric constant as response of dipoles is an indicator of degraded conductivity. This behavior is also referred to decrease of loss by means of dielectric relaxation [42]. Actually, the contribution of interfacial and dipole polarization to dielectric constant decreased at higher frequencies due to the relaxation. Higher doped samples show comparatively lower values of tanδ which slowly decrease with frequency. Higher dielectric loss tangent (dissipation) causes to high electric conductivity (high leakage current). Comparatively higher value of dielectric loss at initial frequency range is related to the resonance of the defect dipoles.

3.4. Magnetic properties

Magnetic behavior of the samples is presented in Figure 7. Influence of Gd substitution is monitored by measuring magnetization vs. field (M-H). As shown in the magnified part of the figure, hysteresis loops of BFO and 1 Gd samples point out antiferromagnetic behavior. However, those of the samples ranged from 3 to 15 according to Gd ratio show non-saturated ferromagnetic behavior with significant remnant magnetization and coercive field. These results are compatible with those of our previous results of up to 5% Gd ratio [44]. Furthermore, the double remanent magnetization of 10% Gd ratio was measured as high as 0.3 emu/g. This behavior indicates the boost of magnetic properties by Gd substitution. Substantial increase of magnetization is correlated with increase of Gd ratio as following possible reasons. Different magnetic moments of Gd and Fe lead to interrupt the spiral spin structure. Moreover, because of the remarkable ionic size difference and bonding parameters of Gd and Fe superexchange interaction is perturbed. Furthermore, variation of the bond angle and the bond length of Gd-O-Fe cause to collapse spin cyloid structure. Structural distortion due to ion substitution results in canting of spins, changing of Fe-O-Fe angle and length [45], collapsing and suppression of spin cycloid structure [46]. For instance, significant

ionic size difference between the host and substitution ions results in large lattice distortion which causes to change bond length and bond angle. Based on the calculation, Goldschmidt tolerance factor decreases with increase of substitution of Gd ratio. This indicates distortion in perovskite structure subsequent change in bond length and bond angle [45]. Furthermore, in the case of structural change the spin cycloid structure would collapse [47]. Increase in coercive field by increasing Gd ratio is ascribed with lowered domain size and allowable formation of inhomogeneous domain via structural transition.

4. Conclusions

In conclusion, modification of critical chemical composition of $BiFeO_3$ by means of substitutions of La for Bi and Gd for Fe sites was successfully carried out to enhance multiferroic properties. By keeping La ratio at 10 mol % and increasing Gd ratio from 1 to 15 mol % crystal structural, microstructure, dielectric behavior and magnetic properties were observed. Regarding Gd ratio, up to 5 mol% rhombohedral phase is successfully obtained. Higher substitution causes to transition of crystal structure of rhombohedral to orthorhombic phase. It was measured that relative permittivity and dielectric loss diminish with rising Gd ratio. Especially, that Gd having different magnetic moment and larger ionic radius is successfully substituted for Fe site of $BiFeO_3$ causes to improve magnetic properties by expense of structural modification. It was concluded that the magnetic properties were significantly boost by increasing Gd ratio. This behavior is correlated with the variation of magnetic properties upon structural modification and collapse of cycloid spin structure of BFO.

Acknowledgments

The Scientific and Technological Research Council of Turkey (TUBITAK) is acknowledged by the corresponding author, Mehmet S. Bozgeyik, for postdoctoral scholarship (2219). This research was financial supported by the DOE-Grant#DE-FG02-08ER46526 at the University

of Puerto Rico (UPR). The conducted research is partially financially supported by the Scientific Research Project of 2018/2-51M of Kahramanmaras Sutcu Imam University.

References:

[1] S. Fusil, V. Garcia, A. Barthelemy, and M. Bibes, *Magnetoelectric Devices for Spintronics*, Annual Review of Materials Research, Vol 44 44 (2014), pp. 91-116.

[2] M. Bibes, and A. Barthelemy, *Multiferroics: Towards a magnetoelectric memory*, Nature Materials 7 (2008), pp. 425-426.

[3] I. Busch-Vishniac, *Trends in electromechanical transduction*, The Journal of the Acoustical Society of America 103 (1998), pp. 2860-2860.

[4] W. Eerenstein, N.D. Mathur, and J.F. Scott, *Multiferroic and magnetoelectric materials*, Nature 442 (2006), pp. 759-765.

[5] N. Fujimura, T. Ishida, T. Yoshimura, and T. Ito, *Epitaxially grown YMnO3 film: New candidate for nonvolatile memory devices*, Applied Physics Letters 69 (1996), pp. 1011-1013.

[6] R. Ramesh, and N.A. Spaldin, *Multiferroics: progress and prospects in thin films*, Nature Materials 6 (2007), pp. 21-29.

[7] V.E. Wood, A. Austin, A. Freeman, and H. Schmid, *Magnetoelectric interaction phenomena in crystals*, Gordon and Breach, London (1975).

[8] H. Zheng, Q. Zhan, F. Zavaliche, M. Sherburne, F. Straub, M.P. Cruz, L.Q. Chen, U. Dahmen, and R. Ramesh, *Controlling self-assembled perovskite-spinel nanostructures*, Nano Letters 6 (2006), pp. 1401-1407.

[9] W. Cai, R.L. Gao, C.L. Fu, L.W. Yao, G. Chen, X.L. Deng, Z.H. Wang, X.L. Cao, and F.Q. Wang, *Microstructure, enhanced electric and magnetic properties of Bi-o.9 La0.1FeO3 ceramics prepared by microwave sintering*, Journal of Alloys and Compounds 774 (2019), pp. 61-68.

[10] O. Polat, M. Coskun, F.M. Coskun, Z. Durmus, M. Caglar, and A. Turut, *Os doped YMnO3 multiferroic: A study investigating the electrical properties through tuning the doping level*, Journal of Alloys and Compounds 752 (2018), pp. 274-288.

[11] W. Prellier, M.P. Singh, and P. Murugavel, *The single-phase multiferroic oxides: from bulk to thin film (vol 17, pg 803, 2005)*, Journal of Physics-Condensed Matter 17 (2005), pp. 7753-7753.

[12] F. Kubel, and H. Schmid, *Structure of a ferroelectric and ferroelastic monodomain crystal of the perovskite BiFeO3*, Acta Crystallographica Section B: Structural Science 46 (1990), pp. 698-702.

[13] E. Palaimiene, J. Macutkevic, D.V. Karpinsky, A.L. Kholkin, and J. Banys, *Dielectric investigations of polycrystalline samarium bismuth ferrite ceramic*, Applied Physics Letters 106 (2015).

[14] B. Ruette, S. Zvyagin, A.P. Pyatakov, A. Bush, J.F. Li, V.I. Belotelov, A.K. Zvezdin, and D. Viehland, *Magnetic-field-induced phase transition in BiFeO3 observed by high-field electron spin resonance: Cycloidal to homogeneous spin order*, Physical Review B 69 (2004).

[15] T.D. Rao, and S. Asthana, *Evidence of improved ferroelectric phase stabilization in Nd and Sc co-substituted BiFeO3*, Journal of Applied Physics 116 (2014).

[16] J. Wang, J.B. Neaton, H. Zheng, V. Nagarajan, S.B. Ogale, B. Liu, D. Viehland, V. Vaithyanathan, D.G. Schlom, U.V. Waghmare, N.A. Spaldin, K.M. Rabe, M. Wuttig, and R. Ramesh, *Epitaxial BiFeO3 multiferroic thin film heterostructures*, Science 299 (2003), pp. 1719-1722.

[17] D.H. Kuang, P. Tang, S.H. Yang, and Y.L. Zhang, *Thickness dependent ferroelectric and magnetic properties of Bi0.9Gd0.1Fe0.9Co0.1O3 films prepared by RF magnetron sputtering*, Journal of Magnetism and Magnetic Materials 397 (2016), pp. 33-38.
[18] A.K. Tagantsev, I. Stolichnov, E.L. Colla, and N. Setter, *Polarization fatigue in ferroelectric films: Basic experimental findings, phenomenological scenarios, and microscopic features*, Journal of Applied Physics 90 (2001), pp. 1387-1402.
[19] C. Ederer, and N.A. Spaldin, *Weak ferromagnetism and magnetoelectric coupling in bismuth ferrite*, Physical Review B 71 (2005).
[20] M. Kumar, and K.L. Yadav, *Study of room temperature magnetoelectric coupling in Ti substituted bismuth ferrite system*, Journal of Applied Physics 100 (2006).
[21] X.D. Qi, J. Dho, R. Tomov, M.G. Blamire, and J.L. MacManus-Driscoll, *Greatly reduced leakage current and conduction mechanism in aliovalent-ion-doped BiFeO3*, Applied Physics Letters 86 (2005).
[22] C. Tabares-Muñoz, J.-P. Rivera, A. Bezinges, A. Monnier, and H. Schmid, *Measurement of the quadratic magnetoelectric effect on single crystalline BiFeO3*, Japanese Journal of Applied Physics 24 (1985), p. 1051.
[23] R. Przenioslo, M. Regulski, and I. Sosnowska, *Modulation in multiferroic BiFeO3: Cycloidal, elliptical or SDW?*, Journal of the Physical Society of Japan 75 (2006).
[24] I. Sosnowska, T. Peterlinneumaier, and E. Steichele, *Spiral Magnetic-Ordering in Bismuth Ferrite*, Journal of Physics C-Solid State Physics 15 (1982), pp. 4835-4846.
[25] K.S. Nalwa, and A. Garg, *Phase evolution, magnetic and electrical properties in Sm-doped bismuth ferrite*, Journal of Applied Physics 103 (2008).
[26] K.F. Wang, J.M. Liu, and Z.F. Ren, *Multiferroicity: the coupling between magnetic and polarization orders*, Advances in Physics 58 (2009), pp. 321-448.
[27] P. Yang, K.M. Kim, Y.G. Joh, D.H. Kim, J.Y. Lee, J. Zhu, and H.Y. Lee, *Effect of BaTiO3 buffer layer on multiferroic properties of BiFeO3 thin films*, Journal of Applied Physics 105 (2009).
[28] V.A. Khomchenko, D.A. Kiselev, M. Kopcewicz, M. Maglione, V.V. Shvartsman, P. Borisov, W. Kleemann, A.M.L. Lopes, Y.G. Pogorelov, J.P. Araujo, R.M. Rubinger, N.A. Sobolev, J.M. Vieira, and A.L. Kholkin, *Doping strategies for increased performance in BiFeO3*, Journal of Magnetism and Magnetic Materials 321 (2009), pp. 1692-1698.
[29] T.J. Park, G.C. Papaefthymiou, A.J. Viescas, Y. Lee, H. Zhou, and S.S. Wong, *Composition-dependent magnetic properties of BiFeO3-BaTiO3 solid solution nanostructures*, Physical Review B 82 (2010).
[30] M.S. Bozgeyik, J.S. Cross, H. Ishiwara, and K. Shinozaki, *Electrical and memory window properties of Sr0.8-xBaxBi2.2Ta2-yZryO9 ferroelectric gate in metal-ferroelectric-insulator-semiconductor structure*, Journal of Electroceramics 28 (2012), pp. 158-164.
[31] Y.K. Jun, W.T. Moon, C.M. Chang, H.S. Kim, H.S. Ryu, J.W. Kim, K.H. Kim, and S.H. Hong, *Effects of Nb-doping on electric and magnetic properties in multi-ferroic BiFeO3 ceramics*, Solid State Communications 135 (2005), pp. 133-137.
[32] V.R. Palkar, D.C. Kundaliya, S.K. Malik, and S. Bhattacharya, *Magnetoelectricity at room temperature in the Bi0.9-xTbxLa0.1FeO3 system*, Physical Review B 69 (2004).
[33] V.R. Palkar, and K. Prashanthi, *Observation of magnetoelectric coupling in Bi(0.7)Dy(0.3)FeO(3) thin films at room temperature*, Applied Physics Letters 93 (2008).
[34] Z. Cheng, A. Li, X. Wang, S.X. Dou, K. Ozawa, H. Kimura, S. Zhang, and T.R. Shrout, *Structure, ferroelectric properties, and magnetic properties of the La-doped bismuth ferrite*, (2008).
[35] Q.H. Jiang, C.W. Nan, and Z.J. Shen, *Synthesis and properties of multiferroic La-modified BiFeO3 ceramics*, Journal of the American Ceramic Society 89 (2006), pp. 2123-2127.
[36] Y.R. Song, F. Yang, M.Y. Yao, F.F. Zhu, L. Miao, J.P. Xu, M.X. Wang, H. Li, X. Yao, F.H. Ji, S. Qiao, Z. Sun, G.B. Zhang, B. Gao, C.H. Liu, D. Qian, C.L. Gao, and J.F. Jia, *Large magnetic moment of gadolinium substituted topological insulator: Bi1.98Gd0.02Se3*, Applied Physics Letters 100 (2012).

[37] R.t. Shannon, *Revised effective ionic radii and systematic studies of interatomic distances in halides and chalcogenides*, Acta Crystallographica Section A: Crystal Physics, Diffraction, Theoretical and General Crystallography 32 (1976), pp. 751-767.
[38] G. Arya, R.K. Kotnala, and N.S. Negi, *A Novel Approach to Improve Properties of BiFeO3 Nanomultiferroics*, Journal of the American Ceramic Society 97 (2014), pp. 1475-1480.
[39] A.Z. Simoes, E.C. Aguiar, A.H.M. Gonzalez, J. Andres, E. Longo, and J.A. Varela, *Strain behavior of lanthanum modified BiFeO3 thin films prepared via soft chemical method*, Journal of Applied Physics 104 (2008).
[40] Z.B. Xing, X.H. Zhu, J.M. Zhu, Z.G. Liu, and T. Al-Kassab, *Structural, Raman, and Dielectric Studies on Multiferroic Mn-doped Bi1-xLaxFeO3 Ceramics*, Journal of the American Ceramic Society 97 (2014), pp. 2323-2330.
[41] K. Sen, K. Singh, A. Gautam, and M. Singh, *Dispersion studies of La substitution on dielectric and ferroelectric properties of multiferroic BiFeO3 ceramic*, Ceramics International 38 (2012), pp. 243-249.
[42] B. Yotburut, P. Thongbai, T. Yamwong, and S. Maensiri, *Electrical and nonlinear current-voltage characteristics of La-doped BiFeO3 ceramics*, Ceramics International 43 (2017), pp. 5616-5627.
[43] F.G. Chang, N. Zhang, F. Yang, S.X. Wang, and G.L. Song, *Effect of Cr substitution on the structure and electrical properties of BiFeO3 ceramics*, Journal of Physics D-Applied Physics 40 (2007), pp. 7799-7803.
[44] M.S. Bozgeyik, R.K. Katiyar, and R.S. Katiyar, *Improved magnetic properties of bismuth ferrite ceramics by La and Gd co-substitution*, Journal of Electroceramics 40 (2018), pp. 247-256.
[45] S.M.A. Kader, D.E.J. Ruth, M.V.G. Babu, M. Muneeswaran, N.V. Giridharan, and B. Sundarakannan, *Investigations on the effect of Ba and Zr co-doping on the structural, thermal, electrical and magnetic properties of BiFeO3 multiferroics*, Ceramics International 43 (2017), pp. 15544-15550.
[46] A. Tamilselvan, S. Balakumar, M. Sakar, C. Nayek, P. Murugavel, and K.S. Kumar, *Role of oxygen vacancy and Fe-O-Fe bond angle in compositional, magnetic, and dielectric relaxation on Eu-substituted BiFeO3 nanoparticles*, Dalton Transactions 43 (2014), pp. 5731-5738.
[47] R.Q. Guo, L. Fang, W. Dong, F.G. Zheng, and M.R. Shen, *Enhanced Photocatalytic Activity and Ferromagnetism in Gd Doped BiFeO3 Nanoparticles*, Journal of Physical Chemistry C 114 (2010), pp. 21390-21396.

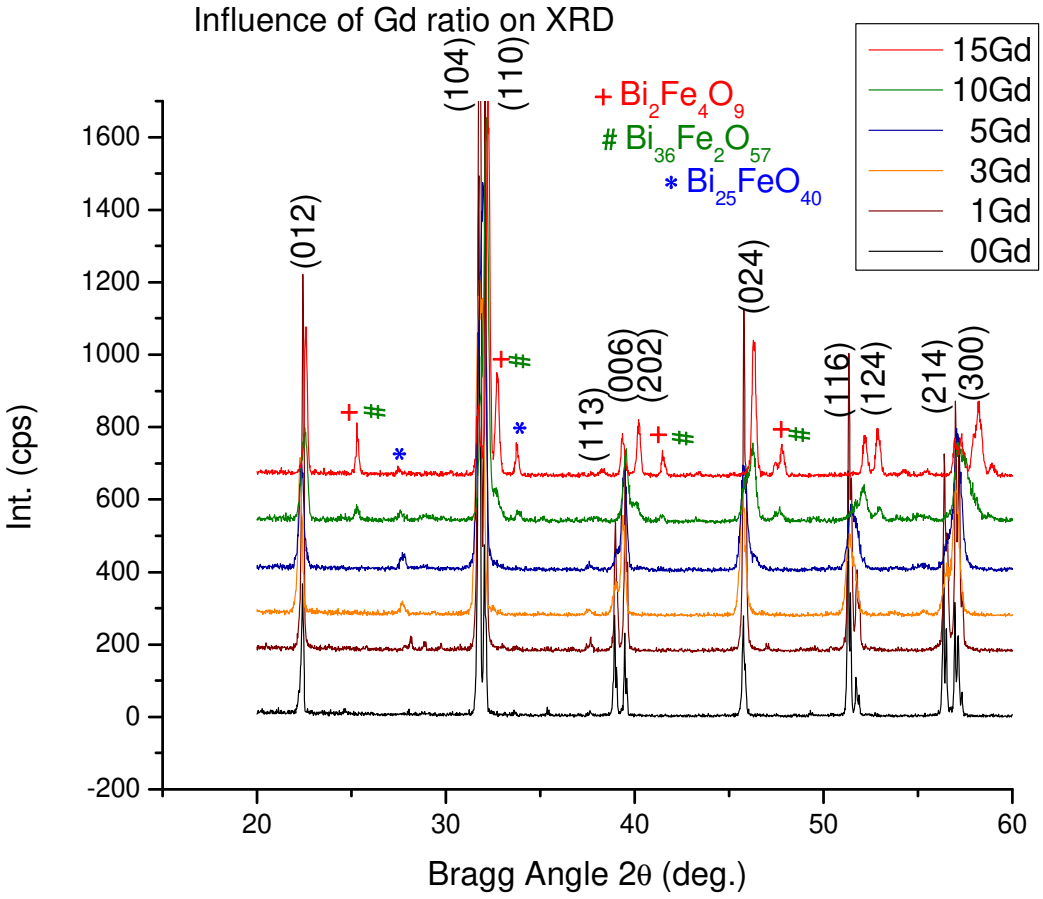

Figure 1. Comparison of XRD patterns of ascending Gd but fixed La ratio of BFO samples.

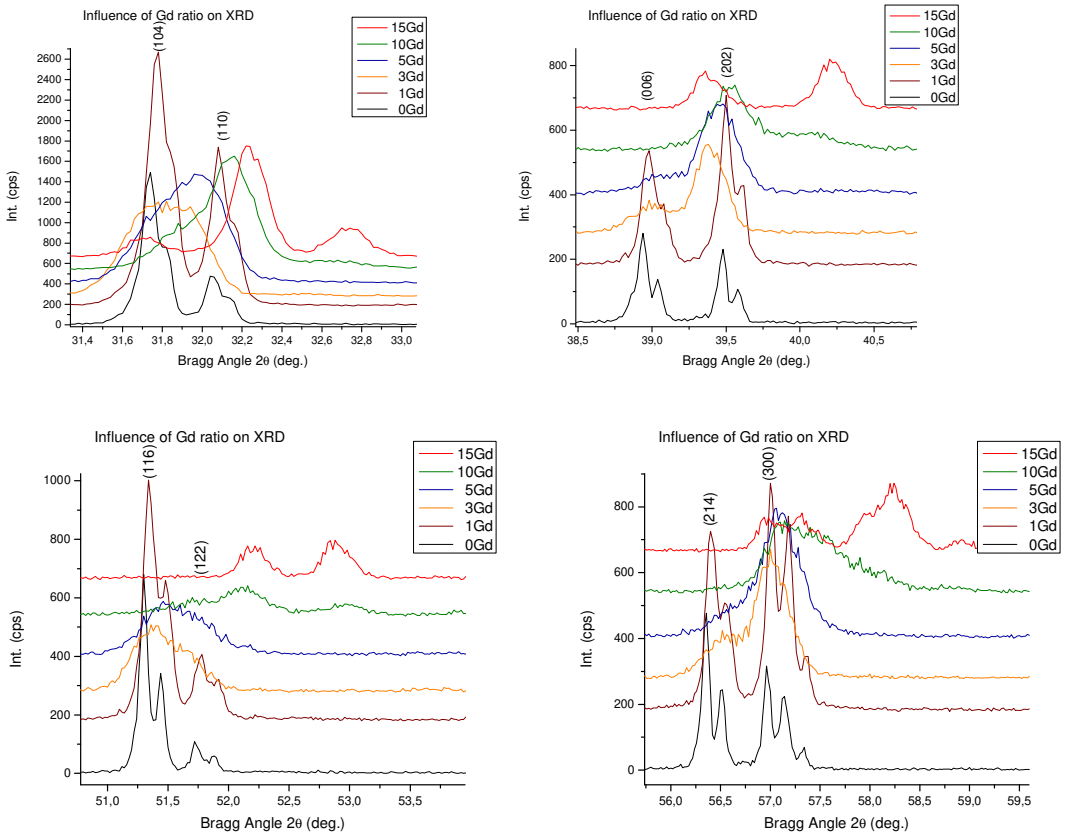

Figure 2. Magnified XRD patterns shown in Figure 1.

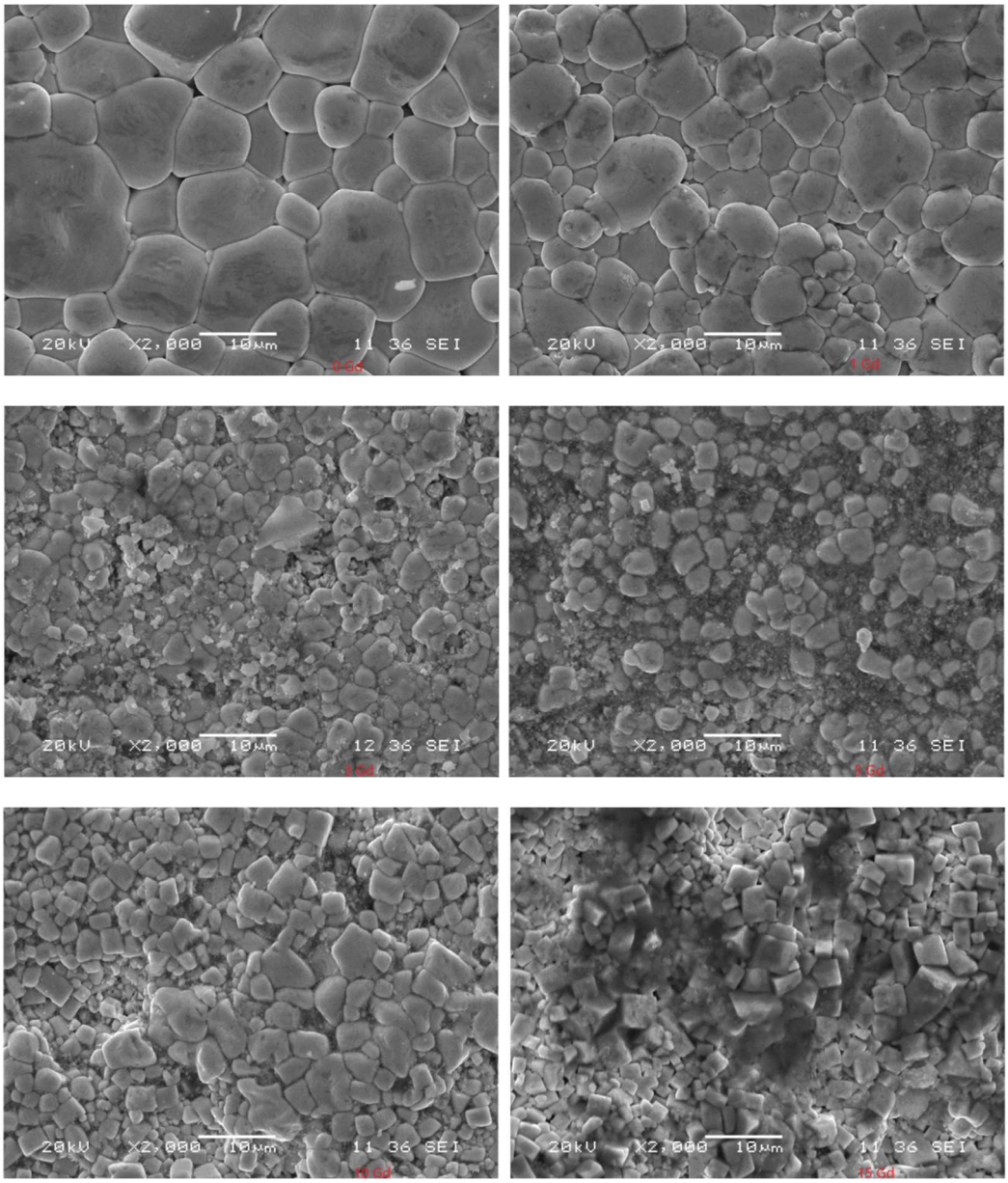

Figure 3. Observation of the microstructural variation of La modified BFO by increasing Gd ratio.

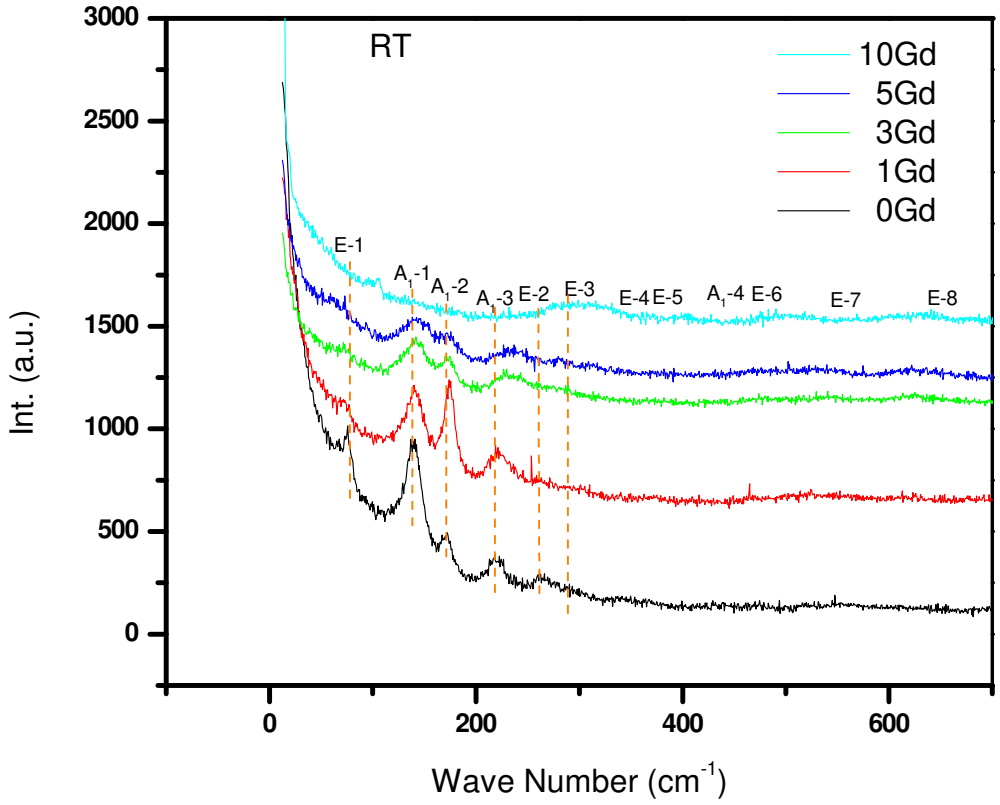

Figure 4. Comparing room temperature Raman spectra of La modified BFO with enhancing Gd ratio.

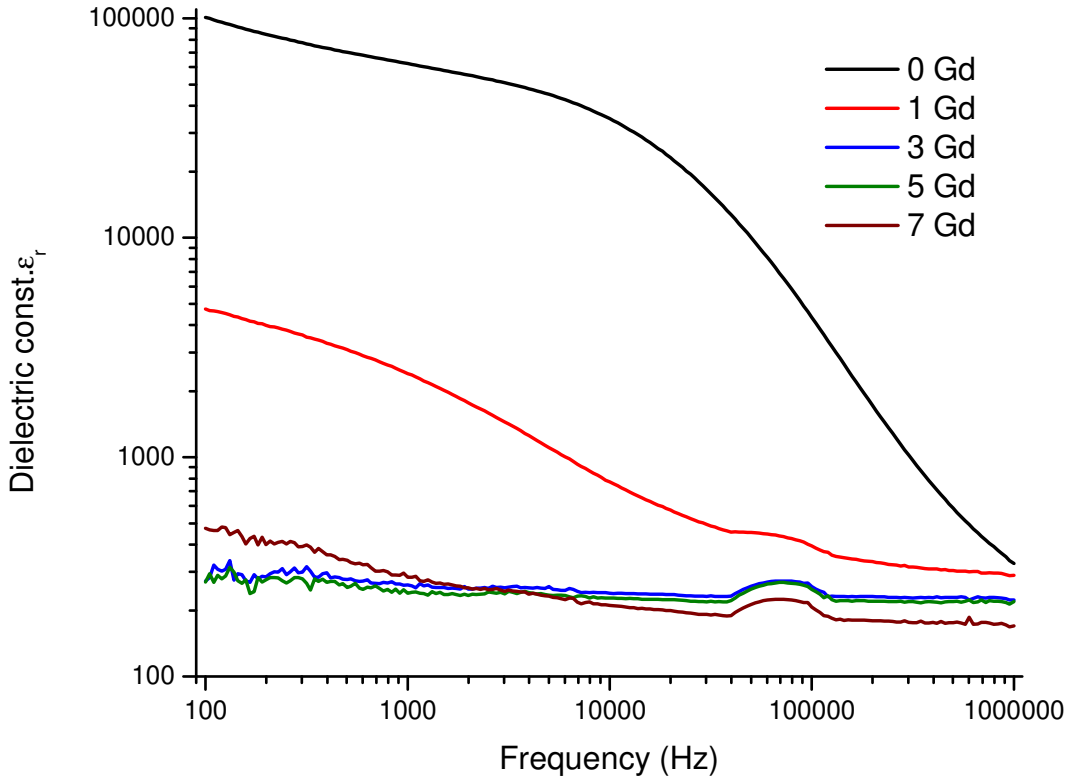

Figure 5. Influence of ascending Gd ratio on the dielectric constant of La modified BFO.

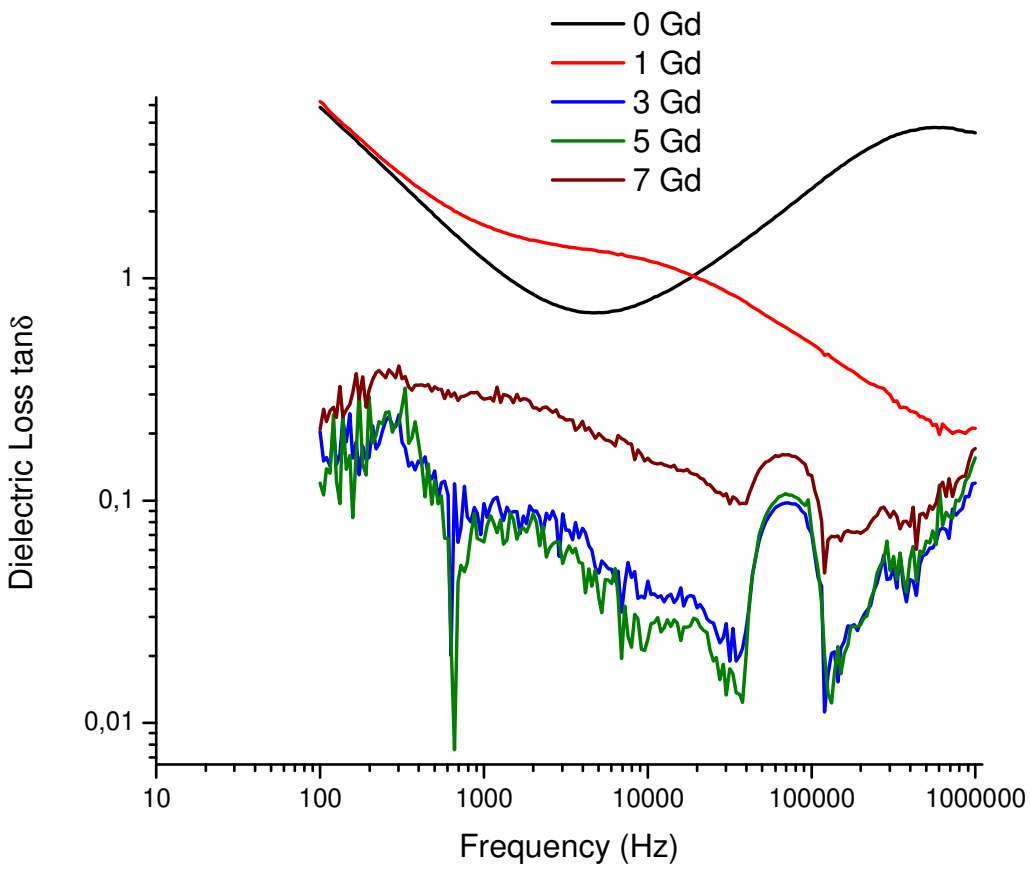

Figure 6. Comparing the dielectric loss by increasing Gd ratio of the La modified BFO.

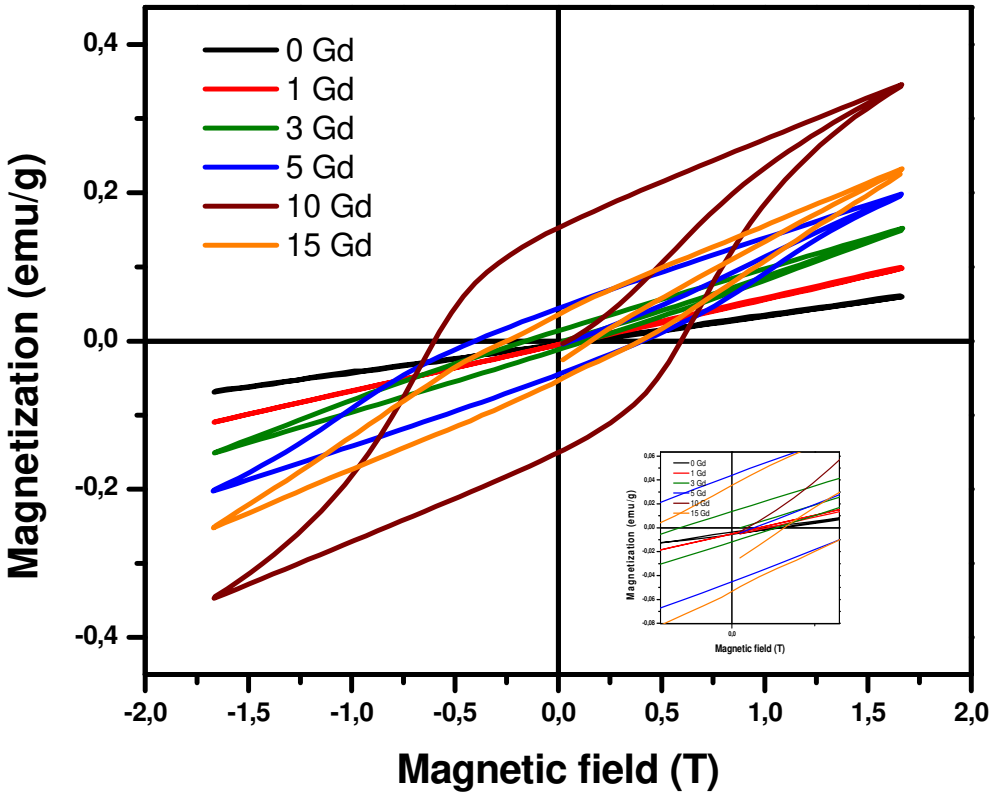

Figure 7. Effect of ascending Gd Ratio of La modified BFO on magnetization.

Figure Captions:

Figure 1. Comparison of XRD patterns of ascending Gd but fixed La ratio of BFO samples.

Figure 2. Magnified XRD patterns shown in Figure 1.

Figure 3. Observation of the microstructural variation of La modified BFO by increasing Gd ratio.

Figure 4. Comparing room temperature Raman spectra of La modified BFO with enhancing Gd ratio.

Figure 5. Influence of ascending Gd ratio on the dielectric constant of La modified BFO.

Figure 6. Comparing the dielectric loss by increasing Gd ratio of the La modified BFO.

Figure 7. Effect of ascending Gd Ratio of La modified BFO on magnetization.

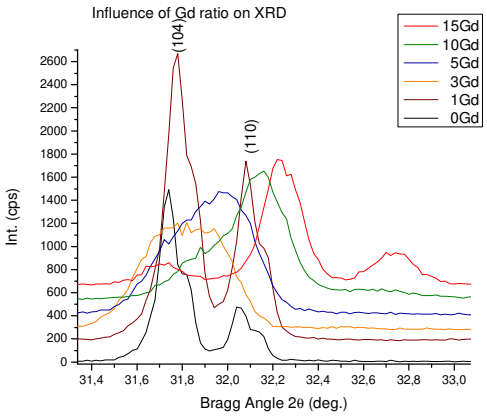
Influence of Gd ratio on XRD
(104)
(110)
15Gd
10Gd
5Gd
3Gd
1Gd
0Gd
Int. (cps)
Bragg Angle 2θ (deg.)

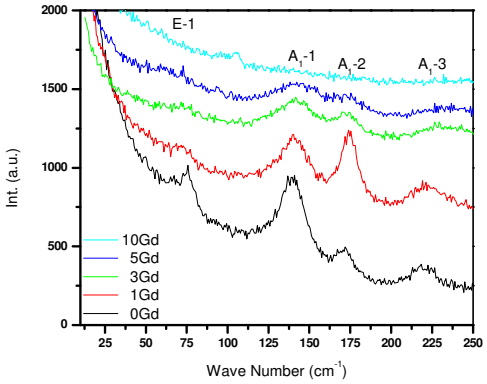
E-1
A1-1
A1-2
A1-3
10Gd
5Gd
3Gd
1Gd
0Gd
Int. (a.u.)
Wave Number (cm-1)

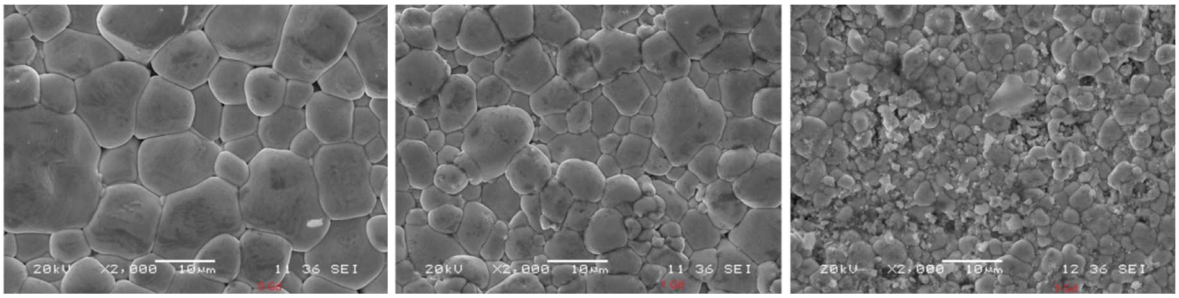

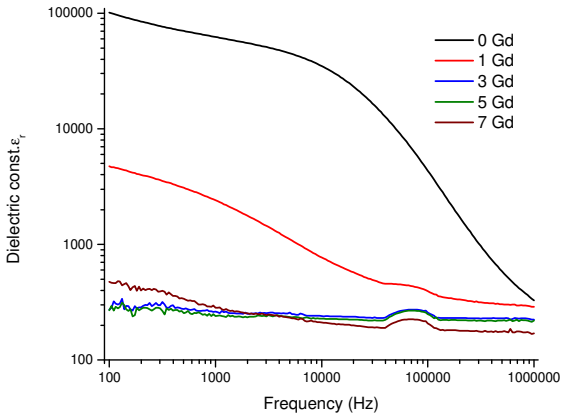
0 Gd
1 Gd
3 Gd
5 Gd
7 Gd
Dielectric const.ε'r
Frequency (Hz)

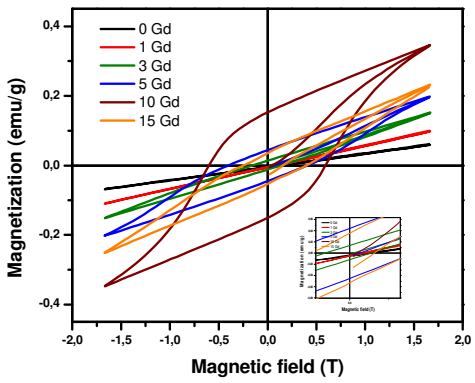
0 Gd
1 Gd
3 Gd
5 Gd
10 Gd
15 Gd
Magnetization (emu/g)
Magnetic field (T)